

# 2D BAO vs 3D BAO: solving the Hubble tension with alternative cosmological models

Sowmaydeep Dwivedi,<sup>1</sup> Marcus Högås<sup>a</sup>

<sup>a</sup>Oskar Klein Centre, Department of Physics, Stockholm University,  
SE-106 91 Stockholm, Sweden

E-mail: [sowmaydeep@gmail.com](mailto:sowmaydeep@gmail.com), [marcus.hogas@fysik.su.se](mailto:marcus.hogas@fysik.su.se)

**Abstract.** Ordinary 3D Baryon Acoustic Oscillations (BAO) data are model-dependent, requiring the assumption of a cosmological model to calculate comoving distances during data reduction. Throughout the present-day literature, the assumed model is  $\Lambda$ CDM. However, this assumption can be inadequate when analyzing alternative cosmologies, potentially biasing the Hubble constant ( $H_0$ ) low, thus contributing to the Hubble tension. To address this issue, we use model-independent 2D BAO data and compare the results to those obtained using 3D BAO data.

As a concrete example, we investigate the cosmological models provided by bimetric gravity, a modified theory of gravity that transitions from a negative cosmological constant in the early universe to a positive one in the late universe. By combining 2D BAO data with cosmic microwave background and type Ia supernovae data, we find that the inverse distance ladder in this theory yields a Hubble constant of  $H_0 = (71.0 \pm 0.9)$  km/s/Mpc, consistent with the SH0ES local distance ladder measurement of  $H_0 = (73.0 \pm 1.0)$  km/s/Mpc. Replacing 2D BAO with 3D BAO results in  $H_0 = (68.6 \pm 0.5)$  km/s/Mpc from the inverse distance ladder. We conclude that the choice of BAO data significantly impacts the Hubble tension, with ordinary 3D BAO data exacerbating the tension, while 2D BAO data provides results consistent with the local distance ladder.

---

<sup>1</sup>Corresponding author.

---

## Contents

<b>1</b>	<b>Introduction</b>	<b>1</b>
<b>2</b>	<b>Bimetric gravity</b>	<b>3</b>
2.1	Historical background	3
2.2	Theory	3
2.3	Cosmology	4
<b>3</b>	<b>Methodology and data</b>	<b>6</b>
3.1	The SH0ES $H_0$ estimate	6
3.2	Cosmic Microwave Background	6
3.3	Type Ia supernovae	8
3.4	Baryon Acoustic Oscillations	8
3.5	Consistency constraints	9
3.6	MCMC sampling	10
<b>4</b>	<b>Results</b>	<b>10</b>
<b>5</b>	<b>Summary and discussion</b>	<b>14</b>
<b>A</b>	<b>Ratio of the scale factors: equation of motion</b>	<b>16</b>
<b>B</b>	<b>Complementary results</b>	<b>16</b>

---

## 1 Introduction

In the early 20th century, the advent of Einstein’s general theory of relativity (GR) revolutionized our understanding of gravity, providing a robust framework that successfully describes a myriad of cosmic phenomena—ranging from the perihelion precession of Mercury to gravitational lensing and the existence of black holes [1]. This, together with the Standard Model of particle physics, has paved the path for the  $\Lambda$  Cold Dark Matter ( $\Lambda$ CDM) model, providing a cosmological framework that accounts for the vast majority of current observations with astonishing precision.

However, as we have entered the era of high-precision cosmology, a handful of tensions has emerged. The most prominent is the Hubble tension which refers to the fact that the local measurement of the Hubble constant significantly exceeds the inferred value from the inverse distance ladder. The most discrepant estimates is between the local  $H_0$  measurement from the SH0ES team,  $H_0 = (73.0 \pm 1.0)$  km/s/Mpc [2], and the inferred value from the inverse distance ladder using *Planck* satellite data,  $H_0 = (67.8 \pm 0.5)$  km/s/Mpc [3]. This amounts to a  $5\sigma$  discrepancy, making it difficult to explain as a mere statistical fluke. Despite diligent searches for possible systematic errors to explain the tension, it has just been increasing during the last decade.

Accordingly, there is an intense discussion in the contemporary literature whether new physics can alleviate the tension. That is, lowering the local distance ladder (SH0ES) value or increasing the inverse distance ladder value. The former can be achieved by postulating a new

gravitational degree of freedom that modifies gravity on galactic and astronomical scales—a fifth force. This results in a recalibration of the cosmic distance ladder, changing the local distance ladder value of  $H_0$  [4–6]. On the other hand, the inferred value of  $H_0$  from the inverse distance ladder assumes a  $\Lambda$ CDM cosmological model. That is, alternative expansion histories can change the inferred value of  $H_0$  which may result in increased consistency with the local distance ladder. This can be achieved by introducing new particles, changing the properties of dark matter or dark energy, or by modifying the theory of gravity itself, see Refs. [7, 8] for some examples. The focus of this paper is on the latter option, and more precisely on the bimetric theory of gravity and its effect on the Hubble tension.

Bimetric gravity is a natural extension of GR, exhibiting a massive spin-2 field in addition to the massless spin-2 field [9, 10]. The theory is observationally viable, as demonstrated in a number of papers [11–29]. Among its virtues is the existence of self-accelerating cosmological solutions where the accelerated expansion of the Universe is a result of the interaction between the two spin-2 fields—no cosmological constant is needed [11, 13, 16, 26, 30–34]. Another interesting feature is that, under certain conditions, the massive spin-2 field provides a dark matter particle [35–37]. The theory is also scientifically tractable in the sense that even the most general version of the theory only introduces four additional theory parameters, which can be constrained observationally.

Nevertheless, bimetric gravity provides a rich spectrum of cosmological expansion histories that can modify the expansion rate both pre- and post-recombination, thus changing the  $H_0$  value inferred from the inverse distance ladder. The effect of bimetric gravity on the Hubble tension was investigated in Ref. [38] for a restricted subclass of models—more precisely, for some special two-parameter models. It was shown that, for this subclass of models, the tension is eased only very slightly.

In the present work however, we do not restrict ourselves to a limited type of submodel but analyze the most general bimetric model. We investigate the effects of combining different data sets and their impact on the Hubble tension. Specifically, we compare the results using ordinary 3D BAO data with the results using transverse 2D BAO data (BAOtr). We infer  $H_0 = (71.0 \pm 0.9)$  km/s/Mpc from the inverse distance ladder when the general bimetric model is fitted with data from the cosmic microwave background (CMB), type Ia supernovae (SNIa), and BAOtr. This is on the  $2\sigma$  border of the SH0ES value for  $H_0$ . Using 3D BAO instead of BAOtr, the inferred value is  $H_0 = (68.6 \pm 0.5)$  km/s/Mpc, representing only a slight ease of the tension, being in the  $4.4\sigma$  tail of the SH0ES value. The disparate result of BAOtr compared with 3D BAO suggests that the cosmological model dependence in ordinary 3D BAO data may bias  $H_0$  to a low value.

**Notation.** Unless stated otherwise, we use geometrized units where the speed of light and Newton’s gravitational constant are unity,  $c = G = 1$ . In this case, length, time, and mass all have the same units  $L = T = M$ . Geometrical quantities pertaining to the second metric  $f_{\mu\nu}$  are denoted by tildes—if not, then pertaining to the physical metric  $g_{\mu\nu}$ . Derivatives with respect to time are denoted by an overdot, so for example  $\dot{a} = \frac{da}{dt}$ . We let  $\omega_x = \Omega_{x,0}h^2$  where  $h = H_0/(100 \text{ km/s/Mpc})$  is the normalized Hubble constant and  $\Omega_{x,0}$  denotes the present-day density of the species  $x$ . The Hubble constant  $H_0$  is given in units of km/s/Mpc.

## 2 Bimetric gravity

### 2.1 Historical background

Bimetric gravity posits the existence of two dynamical spin-2 fields, or metrics, governing gravitational interactions. The first steps towards the present-day, ghost-free, formulation of this theory was taken by Fierz and Pauli in 1939 [39]. They formulated a consistent linearized theory for a freely propagating massive spin-2 field in Minkowski space-time. However, in 1972 Boulware and Deser examined the coherence of a broad range of nonlinear extensions of this theory. Their conclusion was that the introduction of an additional propagating ghost-like scalar mode is unavoidable in any nonlinear extension of the theory [40]. Nevertheless, building upon works by de Rham, Gabadadze, and Tolley [41–46], in 2011 Hassan and Rosen formulated the ghost-free version of bimetric gravity with two dynamical metrics (spin-2 fields) [9, 47, 48]. This marked the rebirth of massive gravity which has been intensely studied since.

### 2.2 Theory

The ghost-free action for bimetric gravity reads

$$\mathcal{S}_{\text{HR}} = \int d^4x \left[ \frac{1}{2\kappa_g} \sqrt{-\det g} R + \frac{1}{2\kappa_f} \sqrt{-\det f} \tilde{R} - \sqrt{-\det g} \sum_{n=0}^4 \beta_n e_n(S) + \sqrt{-\det g} \mathcal{L}_m + \sqrt{-\det f} \tilde{\mathcal{L}}_m \right]. \quad (2.1)$$

In the action,  $g_{\mu\nu}$  and  $f_{\mu\nu}$  are the two metrics (spin-2 fields) and  $R$  and  $\tilde{R}$  are the corresponding Ricci scalars. The two metrics are dynamical with each metric exhibiting an Einstein–Hilbert term,  $\kappa_g = 8\pi G/c^4$  represents the gravitational constant for  $g_{\mu\nu}$ , while  $\kappa_f$  denotes the gravitational constant for  $f_{\mu\nu}$ . The Lagrangians  $\mathcal{L}_m$  and  $\tilde{\mathcal{L}}_m$  characterize two independent matter sectors coupled to  $g_{\mu\nu}$  and  $f_{\mu\nu}$ , respectively [49, 50]. For simplicity, we only consider matter fields coupled to  $g_{\mu\nu}$  (i.e., assuming  $\tilde{\mathcal{L}}_m = 0$ ), which we accordingly identify as the physical metric, determining the geodesics of freely falling observers. Further, the elementary symmetric polynomials of the square root ( $S$ ) of the two metrics, denoted by  $e_n(S)$  in (2.1), are,

$$\begin{aligned} e_0(S) &= 1, & e_1(S) &= [S], & e_2(S) &= \frac{1}{2}([S]^2 - [S^2]), \\ e_3(S) &= \frac{1}{6}([S]^3 - 3[S^2][S] + 2[S^3]), & e_4(S) &= \det(S). \end{aligned} \quad (2.2)$$

In (2.2),  $[S] = \text{Tr } S$ . The square root of the two metrics,  $S$ , is defined by the equation  $S^\mu{}_\rho S^\rho{}_\nu = g^{\mu\rho} f_{\rho\nu}$  [51, 52].<sup>1</sup> The five coefficients  $\beta_n$  of the polynomials  $e_n(S)$  are constants with the dimension of curvature  $1/L^2$  with  $\beta_1, \beta_2$ , and  $\beta_3$  determining the interaction between the two metrics and  $\beta_0$  and  $\beta_4$  contributing with a cosmological constant to the  $g$ -metric and  $f$ -metric, respectively.

As opposed to some other modified gravity theories such as Horndeski theory [53], bimetric gravity features a finite number of theory parameters which makes the theory scientifically tractable, with the possibility to falsify the theory and constrain the theory parameters. As

---

<sup>1</sup>Note that this equation has no unique solution generically. However, in Ref. [51] it was argued that the principal square root is the appropriate solution as it guarantees a sensible space-time interpretation of the theory.

they stand the  $\beta$ -parameters cannot be constrained by observations due to their invariance under the rescaling

$$(f_{\mu\nu}, \kappa_f, \beta_n) \rightarrow (\omega f_{\mu\nu}, \omega \kappa_f, \omega^{-n/2} \beta_n), \quad (2.3)$$

with  $\omega$  being an arbitrary constant. Therefore, rescaling-invariant parameters are introduced [23, 26] as

$$B_n \equiv \frac{\kappa_g \beta_n c^n}{H_0^2}. \quad (2.4)$$

Here,  $c$  is the proportionality constant between the metrics in the final de Sitter phase in the cosmological infinite future where  $f_{\mu\nu} = c^2 g_{\mu\nu}$ . For more details, see Refs. [26, 29]. The Hubble constant  $H_0$  is included in the definition of  $B_n$  to render the  $B_n$ -parameters dimensionless. Due to the  $B_n$ -parameters being invariant under the rescaling, they can be observationally constrained.

To enable an intuitive interpretation, we reparameterize from  $(B_0, B_1, B_2, B_3, B_4)$  to what we refer to as the physical parameters  $(\theta, m_{\text{FP}}, \Omega_\Lambda, \alpha, \beta)$ , defined by,

$$\tan^2 \theta = \frac{B_1 + 3B_2 + 3B_3 + B_4}{B_0 + 3B_1 + 3B_2 + B_3}, \quad (2.5a)$$

$$m_{\text{FP}}^2 = \frac{B_1 + 2B_2 + B_3}{\sin^2 \theta}, \quad (2.5b)$$

$$\Omega_\Lambda = \frac{B_0}{3} + B_1 + B_2 + \frac{B_3}{3}, \quad (2.5c)$$

$$\alpha = -\frac{B_2 + B_3}{B_1 + 2B_2 + B_3}, \quad (2.5d)$$

$$\beta = \frac{B_3}{B_1 + 2B_2 + B_3}. \quad (2.5e)$$

As implied by their name, the physical parameters carry specific interpretations. Firstly, the mixing angle  $\theta \in [0, \pi/2]$  governs the mixing of the massive and massless spin-2 fields, also known as mass eigenstates. In the limit  $\theta \rightarrow 0$ , GR is retained whereas in the limit  $\theta \rightarrow \pi/2$ , dRGT massive gravity is retained. The parameter  $m_{\text{FP}}$  represents the mass of the massive spin-2 field. The effective cosmological constant in the final de Sitter phase in the Universe's expansion history is denoted by  $\Omega_\Lambda$ . Lastly, the parameters  $\alpha$  and  $\beta$  play a crucial role in determining the Vainshtein screening mechanism that is responsible for recovering GR results on solar-system scales.

### 2.3 Cosmology

From the Hassan–Rosen action (2.1), one can derive the Friedmann equation governing the evolution of a homogeneous and isotropic universe, as a function of the redshift  $z$ ,

$$\left(\frac{H(z)}{H_0}\right)^2 = \Omega_m(z) + \Omega_r(z) + \Omega_{\text{DE}}(z). \quad (2.6)$$

Here, we have set the spatial curvature to zero,  $\Omega_k = 0$ .  $H = \dot{a}/a$  is the Hubble parameter with  $a$  being the scale factor of the physical metric and  $H_0$  is the present-day value of  $H$ , that is, the Hubble constant. Further,  $\Omega_m$  and  $\Omega_r$  denote the energy density of matter and radiation, respectively, both measured in units of the present-day critical energy density.

What distinguishes eq. (2.6) from the ordinary Friedmann equation of the  $\Lambda$ CDM model is the last term,  $\Omega_{\text{DE}}$ , which results from the interaction between the two metrics. It reads,

$$\Omega_{\text{DE}}(z) = \Omega_{\Lambda} - \sin^2 \theta m_{\text{FP}}^2 [1 - y(z)] \left[ 1 + \alpha(1 - y(z)) + \frac{\beta}{3}(1 - y(z))^2 \right], \quad (2.7)$$

where  $y \equiv \tilde{a}/a$  is the ratio of the scale factors of the two metrics. The first term,  $\Omega_{\Lambda}$ , gives a cosmological constant contribution whereas the remaining terms give a dynamical contribution that evolves with the redshift  $z$ .

From the conservation equations of matter and radiation it follows that,

$$\Omega_m(z) = \Omega_{m,0}(1+z)^3, \quad \Omega_r(z) = \Omega_{r,0}(1+z)^4, \quad (2.8)$$

with  $\Omega_{m,0}$  and  $\Omega_{r,0}$  being the present-day matter density and radiation density, respectively. Finally, an equation can be derived for  $y$  in form of a quartic polynomial in  $y$ . The full expression is shown in eq. (A.1).

With  $y$  being a solution to a quartic polynomial, there are up to four real solutions. Here, we choose the solution which is commonly referred to as the ‘‘finite branch’’. This branch guarantees the absence of the Higuchi ghost and allows for a screening mechanism that restores GR on solar-system scales [26, 54–57]. This branch has a finite range in  $y$ , starting with  $y = 0$  at the Big Bang, then monotonically increasing until  $y = 1$  is reached in the infinite future, that is, in the final de Sitter phase.

In the early-time limit  $z \rightarrow \infty$ , one can show that the bimetric contribution to the Friedmann equation,  $\Omega_{\text{DE}}$ , generically assumes the form of a cosmological constant with magnitude

$$\Omega_{\text{DE}}|_{z \rightarrow \infty} = \Omega_{\Lambda} - \sin^2 \theta m_{\text{FP}}^2 \left( 1 + \alpha + \frac{\beta}{3} \right). \quad (2.9)$$

That is, at early times the background evolution of the Universe is according to a  $\Lambda$ CDM model with a value of the, possibly negative, cosmological constant that is given by eq. (2.9) [26]. In the infinite future, the Universe approaches a de Sitter phase where the cosmological constant is set by  $\Omega_{\Lambda}$  [26]. So, bimetric cosmology exhibits two  $\Lambda$ CDM phases with generically different cosmological constants, one in the early universe and one in the the late universe. The redshift ranges of these phases are primarily set by the mass of the massive spin-2 field,  $m_{\text{FP}}$ . In the transition between the two  $\Lambda$ CDM phases, there is a rich spectrum of expansion histories depending on the physical parameters (2.5). One can show that if  $\Omega_{\text{DE}}$  is negative, the equation of state  $w_{\text{DE}} \geq -1$  whereas if  $\Omega_{\text{DE}}$  is positive the equation of state is  $w_{\text{DE}} \leq -1$ . In other words,  $\Omega_{\text{DE}}$  grows with time, thus presenting a phantom dark energy contribution to the Friedmann equation (2.6). However,  $w_{\text{DE}} \rightarrow -1$  fast enough in the late universe, thus avoiding a Big Rip [26, 58].

For completeness, we also note that the so-called minimal theories of bigravity (MTBG) [59] share the cosmological background solutions with bimetric gravity. Thereby, all results that we will present here concerning the influence of bimetric gravity on the Hubble tension, also apply to MTBG.

To enable a statistical data analysis, we must solve the Hubble parameter as a function of redshift  $H(z)$ . This is done by solving the cosmological equations of motion numerically, that is, eqs. (2.6), (2.7), (2.8), (A.1). The value of  $y$  at  $z = 0$  is determined by solving eq. (A.2) numerically, choosing the finite branch solution with  $y_0$  in the range  $0 \leq y_0 \leq 1$ .

Subsequently, this value of  $y_0$  allows the calculation of  $\Omega_{\text{DE},0}$  using eq. (2.7). Further, the application of Friedman’s equation (2.6) at  $z = 0$  yields

$$\Omega_{m,0} = 1 - \Omega_{\text{DE},0} - \Omega_{r,0}, \quad (2.10)$$

since  $\frac{H^2(z)}{H_0^2} \Big|_{z=0} = 1$ , by definition. With  $\Omega_{m,0}$  and  $\Omega_{r,0}$  being determined,<sup>2</sup> the remaining step to obtain  $H(z)$  is to solve eq. (A.1) for  $y$  at each redshift, plugging the solution into eq. (2.7) to determine  $\Omega_{\text{DE}}(z)$  and then finally  $H(z)$  via eq. (2.6).

### 3 Methodology and data

#### 3.1 The SH0ES $H_0$ estimate

The SH0ES team estimate of  $H_0$  is based on a three-rung cosmic distance ladder [2]. In the first rung, the period-luminosity relation (PLR) for Cepheid variable stars [60] is calibrated in three anchor galaxies—the Milky Way (MW), NGC 4258, and the Large Magellanic Cloud (LMC). To calibrate the PLR, the distance to these Cepheids must be known. In the MW, the distances can be estimated geometrically from parallax measurements [61, 62]. The distance to NGC 4258 is estimated from water masers close to the centre of this galaxy [63]. The distance to the LMC is estimated from observations of detached eclipsing binaries [64].

In the second rung, the absolute peak magnitude of type Ia supernovae is calibrated in galaxies hosting both SNIa and Cepheids. In the third rung, SNIa are observed in the Hubble flow which yields the magnitude-redshift relation [65]. With the calibrated value for the absolute SNIa peak magnitude,  $H_0$  is finally obtained from the intercept of the magnitude-redshift relation. The 2022 baseline result from the SH0ES team, fitting all three rungs simultaneously, is  $H_0 = (73.0 \pm 1.0) \text{ km/s/Mpc}$  [2]. This can be used as a prior on  $H_0$  in which case the contribution to the likelihood is given by

$$-2 \ln \mathcal{L}_{\text{SH0ES}} = \left( \frac{H_0^{\text{model}} - 73.0 \text{ km/s/Mpc}}{1.0 \text{ km/s/Mpc}} \right)^2. \quad (3.1)$$

#### 3.2 Cosmic Microwave Background

As the temperature of the Universe had dropped sufficiently, neutral hydrogen was formed and the photons decoupled from the baryon-photon fluid and began to free stream. This is known as recombination, or photon decoupling, and happened at a redshift of  $z_* \simeq 1090$ . Today, we can observe these photons as the cosmic microwave background radiation, carrying the imprint of the fluctuations in the baryon-photon fluid at the last-scattering surface at redshift  $z_*$ .

The *Planck* satellite observations of the temperature fluctuations in the CMB can be used to estimate  $H_0$  [3]. However, this assumes a  $\Lambda$ CDM cosmology. Here, we investigate the inferred value of  $H_0$  in the case of bimetric cosmology. For this purpose, we use the CMB compressed likelihood featuring the three parameters  $(\mathcal{R}, l_A, \omega_b)$ . The “shift parameter”  $\mathcal{R}$  encodes the angular scale of the Hubble horizon at the photon decoupling epoch and is defined by [66]

$$\mathcal{R} = \sqrt{\Omega_{m,0} H_0^2} D_A(z_*). \quad (3.2)$$

---

<sup>2</sup>In Section 3.2, we show how  $\Omega_{r,0}$  is determined from the CMB temperature.

The comoving angular diameter distance  $D_A$  is calculated by

$$D_A(z) = \int_0^z \frac{dz}{H(z)}, \quad (3.3)$$

assuming a spatially flat cosmology. The redshift  $z_*$  of photon decoupling is given by the analytical approximation in Ref. [67].

The sound horizon at photon decoupling  $r_s(z_*)$  defines a standard ruler which is imprinted in the CMB temperature fluctuations. This manifests itself as a maximal correlation between hotspots in the CMB temperature map occurring at the angular scale  $\theta_{\text{CMB}}$ , given by

$$\theta_{\text{CMB}} = r_s(z_*)/d_A(z_*). \quad (3.4)$$

Here,  $d_A = D_A/(1+z)$ . The parameter  $l_A$  is the multipole number corresponding to this angular scale,

$$l_A = \pi D_A(z_*)/r_s(z_*), \quad (3.5)$$

where  $r_s$  is the sound horizon,

$$r_s(z) = \int_z^\infty \frac{c_s(z)}{H(z)} dz, \quad (3.6)$$

and  $c_s$  is the sound speed,

$$c_s = \frac{1}{\sqrt{3 \left(1 + \frac{3\omega_b}{4\omega_\gamma} \frac{1}{1+z}\right)}}. \quad (3.7)$$

The photon energy density  $\omega_\gamma$  can be determined from the CMB temperature via the relation [68]

$$\frac{3}{4\omega_\gamma} = 31500 \left(\frac{2.7 \text{ K}}{T_{\text{CMB}}}\right)^4, \quad T_{\text{CMB}} = 2.7255 \text{ K}. \quad (3.8)$$

The present-day radiation density is set by,

$$\Omega_{r,0} = \Omega_{\gamma,0}(1 + 0.2271 N_{\text{eff}}), \quad (3.9)$$

with  $N_{\text{eff}}$  being the effective number of neutrino species, which we set to  $N_{\text{eff}} = 3.046$  [3].

Finally,

$$\omega_b = \Omega_{b,0} h^2, \quad (3.10)$$

encodes the present-day baryon density.

The latest *Planck* values for  $(\mathcal{R}, l_A, \omega_b)$  are given in Tab. 1 and the CMB likelihood is calculated as,

$$-2 \ln \mathcal{L}_{\text{CMB}} = \sum_{ij} \Delta_i C_{ij}^{-1} \Delta_j. \quad (3.11)$$

Here,  $\Delta$  is the difference between the model prediction and the observed values,

$$\Delta^T = \left( \mathcal{R}^{\text{model}} - \mathcal{R}^{\text{obs}}, l_A^{\text{model}} - l_A^{\text{obs}}, \omega_b^{\text{model}} - \omega_b^{\text{obs}} \right), \quad (3.12)$$

$C^{-1}$  is the inverse covariance matrix and the covariance matrix  $C$  can be read off from the correlation matrix  $\rho$  via the relation  $C_{ij} = \sigma_i \sigma_j \rho_{ij}$  (no summation implied) with  $\sigma_i$  and  $\rho_{ij}$  given in Tab. 1.



	<i>Planck</i>	$\mathcal{R}$	$l_A$	$\omega_b$
$\mathcal{R}$	$1.7493^{+0.0046}_{-0.0047}$	1.0	0.47	-0.66
$l_A$	$301.462^{+0.089}_{-0.090}$	0.47	1.0	-0.34
$\omega_b$	$0.02239 \pm 0.00015$	-0.66	-0.34	1.0

**Table 1:** The 68% CL limits on the CMB compressed likelihood [68]. The last three columns show the correlation matrix  $\rho_{ij}$ .

### 3.3 Type Ia supernovae

Type Ia supernovae are standardizable candles and can thus be used to probe the expansion history of the Universe. Here, we use the Pantheon+ data sample [65], probing the peak apparent magnitude  $m_B$  of 1701 SNIa light curves in the redshift range  $0.001 \leq z \leq 2.26$ . To retain the supernovae in the Hubble flow, we use only those with a redshift greater than 0.023.<sup>3</sup> The model prediction of the peak  $B$ -band magnitude is given by,

$$m_B(z) = \mathcal{M} + 5 \log_{10} \mathcal{D}_L(z), \quad (3.13)$$

where we marginalize over the intercept  $\mathcal{M}$  when calculating the likelihood. For details, see for example Refs. [29, 69]. Further, the dimensionless luminosity distance  $\mathcal{D}_L$  is defined as

$$\mathcal{D}_L(z) = (1+z) \int_0^z \frac{dz}{E(z)} \quad (3.14)$$

and  $E(z)$  is the normalized expansion rate,  $E(z) = H(z)/H_0$ .

### 3.4 Baryon Acoustic Oscillations

The sound horizon of the baryon-photon fluid is not only imprinted in the CMB temperature fluctuations but also in the large-scale structure of matter (baryons). These fluctuations in the matter distribution are known as baryon acoustic oscillations and the angular scale  $\theta_{\text{BAO}}$  corresponding to the typical angular (transverse) separation of galaxies on the sky, at some redshift  $z$ , is given by,

$$\theta_{\text{BAO}}(z) = r_s(z_d)/D_A(z). \quad (3.15)$$

Here,  $r_s(z_d)$  is the sound horizon at the baryon drag epoch which occurred when the baryons were released from the Compton drag of the photons. Due to the excess of photons over baryons, this occurred at a slightly later point in time than the photon decoupling. The redshift of the drag epoch  $z_d$  is calculated using the analytical approximation in Ref. [67] and is  $z_d \simeq 1060$ .

In the standard 3D BAO data reduction, one infers for example  $D_V(z)/r_s(z_d)$ . That is, the ratio of the volume-average distance and the sound horizon at the baryon drag epoch. The volume-average distance is defined as

$$D_V(z) = \sqrt[3]{D_A^2(z) \frac{z}{H(z)}}. \quad (3.16)$$

<sup>3</sup>The data set is available at [https://github.com/PantheonPlusSH0ES/DataRelease/tree/main/Pantheon%2B\\_Data](https://github.com/PantheonPlusSH0ES/DataRelease/tree/main/Pantheon%2B_Data), last checked 2 July 2024.

$z$	0.11	0.236	0.365	0.45	0.47	0.49	0.51	0.53
$\theta_{\text{BAO}}$ [deg]	19.8	9.06	6.33	4.77	5.02	4.99	4.81	4.29
$\sigma_{\text{BAO}}$ [deg]	3.26	0.23	0.22	0.17	0.25	0.21	0.17	0.30
$z$	0.55	0.57	0.59	0.61	0.63	0.65	2.225	
$\theta_{\text{BAO}}$ [deg]	4.25	4.59	4.39	3.85	3.90	3.55	1.77	
$\sigma_{\text{BAO}}$ [deg]	0.25	0.36	0.33	0.31	0.43	0.16	0.31	

**Table 2:** Transversal BAO data (BAOtr). Adopted from Ref. [70].

One can identify the two factors of  $D_A(z)$  as angular distances and  $z/H(z)$  as a radial distance. To infer  $D_V(z)/r_s(z_d)$  from BAO data, one must calculate the 3D fiducial comoving distances, including the radial distance. For the latter, a cosmological model must be assumed, and the universal assumption in the literature is a  $\Lambda$ CDM model. Due to the assumption of a  $\Lambda$ CDM cosmological model in the BAO data reduction, in recent years it has been questioned whether this introduces a bias when considering alternative cosmological models [70–72].

To circumvent this issue, we use the 2D transversal BAO scale (BAOtr) which can be obtained without assuming any fiducial cosmology. Here instead, in the BAO data reduction one calculates the 2-point angular correlation function in thin, non-overlapping, redshift shells to infer  $\theta_{\text{BAO}}(z)$  at a set of redshifts. The price to pay is that the errors grow by roughly one order of magnitude, from  $\sim 1\%$  to  $\sim 10\%$ .

Here, we use 15 measurements of the angular BAO scale  $\theta_{\text{BAO}}$  in the redshift range  $0.11 \leq z \leq 2.225$ , obtained from the Sloan Digital Sky Survey (SDSS) data releases DR7, DR10, DR11, DR12, and DR12Q and compiled in Tab. 2. The likelihood is calculated as,

$$-2 \ln \mathcal{L}_{\text{BAOtr}} = \sum_{i=1}^{15} \left( \frac{\theta_{\text{BAO}}^{\text{model}}(z_i) - \theta_{\text{BAO}}^{\text{obs}}(z_i)}{\sigma_i} \right)^2. \quad (3.17)$$

When using ordinary 3D BAO data to compare with the BAOtr results, we use the data from the SDSS in combination with the Dark Energy Spectroscopic Instrument (DESI) [73].

### 3.5 Consistency constraints

There are some regions in the bimetric parameter space  $(\theta, m_{\text{FP}}, \Omega_\Lambda, \alpha, \beta)$  that must be avoided [26]. First, to have a continuous, real-valued cosmology devoid of the Higuchi ghost, we must restrict the range of possible values of the physical parameters. Second, observations require GR results to be restored on solar-system scales. Thus, there must exist a screening mechanism hiding the extra degrees of freedom on these scales. To ensure the existence of such a mechanism, we must impose additional constraints on the parameter space. Those are presented in Ref. [26] and we refer to these, together with the restrictions imposed by the Higuchi bound, as consistency constraints.

Bimetric submodels are usually defined by setting one or several of the  $B$ -parameters (or, equivalently,  $\beta$ -parameters) to zero. We note that the consistency constraints presented here, together, require that  $B_1$ ,  $B_2$ , and  $B_3$  are all non-zero [26].<sup>4</sup> Thus, the minimal submodel consistent with these constraints is the  $B_1 B_2 B_3$ -model which is the reason why we do not consider submodels with fewer parameters. In the MCMC sampling, we set the likelihood to zero at the points where the consistency constraints are violated.

<sup>4</sup>The  $B$ -parameters can be expressed in terms of the physical parameters by inverting eq. (2.5).

Model parameter:	$H_0$	$\omega_b$	$\theta$	$m_{\text{FP}}$	$\Omega_\Lambda$
Prior:	U[50, 85]	U(0, 1]	U[0, $\frac{\pi}{2}$ ]	U(0, 10 <sup>8</sup> ]	U(0, 1]

**Table 3:** Priors on the free model parameters for the general bimetric model. All priors are uniform, spanning the range indicated in the table. The upper limits of  $\alpha$  and  $\beta$  are set to 100 while their lower limits are effectively set by imposing the consistency constraints, explained in Section 3.5.

Model	CMB+SN+	$H_0$	$\theta$ (rad)	$\Omega_\Lambda$	$\Delta\text{AIC}$	$\Delta\text{BIC}$
$\Lambda\text{CDM}$	BAOtr	$68.9 \pm 0.5$	0	$0.700 \pm 0.006$	0	0
Bimetric	BAOtr	$71.0 \pm 0.9$	$0.16 \pm 0.03$	$0.724 \pm 0.010$	1.1	-19.9
$\Lambda\text{CDM}$	BAOtr+SH0ES	$69.7 \pm 0.5$	0	$0.709 \pm 0.006$	0	0
Bimetric	BAOtr+SH0ES	$71.9 \pm 0.7$	$0.18 \pm 0.02$	$0.732 \pm 0.007$	13.2	-7.8

**Table 4:** Best-fit values and 68% confidence errors for  $H_0$ ,  $\theta$ , and  $\Omega_\Lambda$ . With CMB+SN+BAOtr, the bimetric model exhibits a significant increase in  $H_0$ , thus being consistent with the local distance ladder measurement.  $\Delta\text{BIC}$  is the difference in the Bayesian information criterion for the bimetric model compared with the  $\Lambda\text{CDM}$  model. A positive value of  $\Delta\text{BIC}$  indicates a favoured bimetric model. With  $\Delta\text{BIC}$  being in favour of the  $\Lambda\text{CDM}$  model, the increased number of parameters does not constitute a sufficient improvement in the fit to data, according to this measure.

### 3.6 MCMC sampling

Markov Chain Monte Carlo (MCMC) methods can be employed in sampling complex probability distributions. Its application is particularly prevalent in Bayesian statistics and computational physics. MCMC operates on the principle of constructing a Markov Chain, where each state in the chain represents a possible configuration of model parameters. The transition from one state to the next is governed by a Markov process, ensuring that the next state depends only on the current state. Over time, the chain converges to a stationary distribution, and samples drawn from this distribution provide an approximation of the posterior distribution. We have incorporated the `emcee` Python library [74], providing a robust and parallelized implementation of Goodman and Weare’s affine invariant MCMC ensemble sampling algorithm [75].

## 4 Results

We present the results for the most general bimetric model. The free parameters and their flat prior ranges are presented in Tab. 3. In Fig. 1, we show the 2D marginalized confidence level contours in the  $(H_0, \theta)$ -plane for different combinations of data sets. The 2D marginalized confidence contours in the full parameter space is displayed in Fig. 4. In Appendix B, we also present the results for certain submodels.

In Fig. 1, we see that SN+CMB yields a weakly constrained  $H_0$ , allowing both for “high” values compatible with SH0ES and for “low” values compatible with the standard  $\Lambda\text{CDM}$  inverse distance ladder estimate. With SN+BAOtr+CMB, the inferred value  $H_0 = 71.0 \pm 0.9$

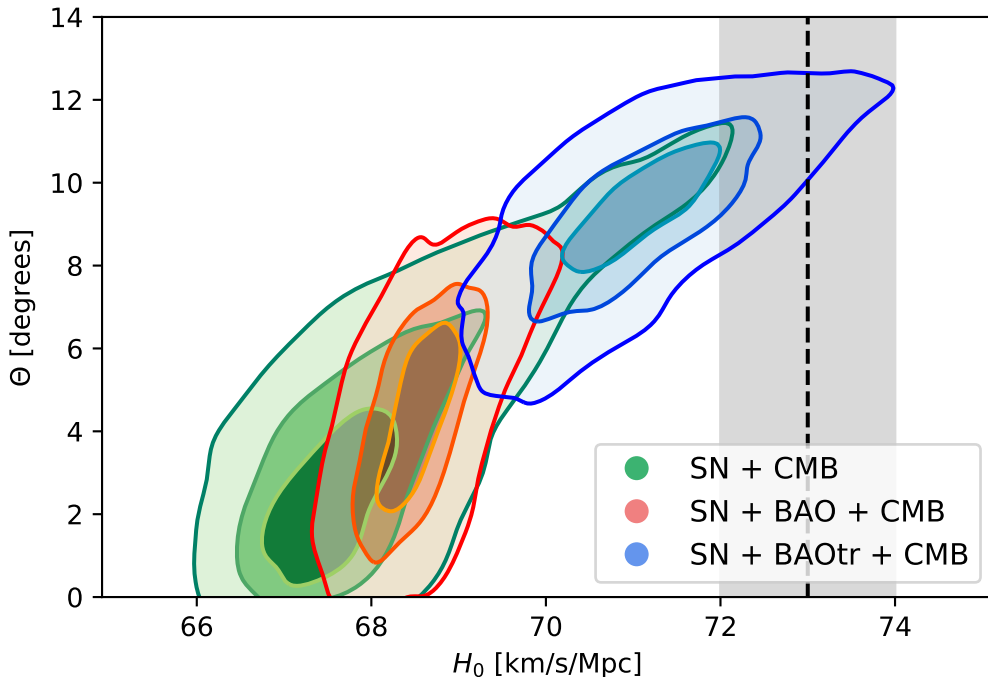


**Figure 1:** 2D marginalized confidence level contours (68 %, 95 %, 99 %) in the  $(H_0, \theta)$ -plane for the general bimetric model. Gray: the SH0ES estimate of  $H_0$ . Green: SN+CMB. With these data sets, the bimetric model yields a wide confidence contour, spanning from “low” values of  $H_0$  to “high” values compatible with SH0ES. Blue: adding BAOtr. Notably, in this case the inferred value of  $H_0$  is consistent with SH0ES. In other words, there is no Hubble tension in bimetric cosmology when BAOtr is used. Red: using ordinary 3D BAO data instead of BAOtr. In this case,  $H_0$  centers around “low” values and a tension in  $H_0$  is manifest.

is consistent with SH0ES. This should be compared with  $H_0 = 68.9 \pm 0.5$ , which is the value obtained when a  $\Lambda$ CDM model is fitted to the same data set. In summary, utilizing transverse BAO data, the Hubble tension is alleviated in bimetric cosmology.

On the other hand, imposing ordinary 3D BAO data instead of BAOtr, there is only a slight increase in  $H_0$  compared with  $\Lambda$ CDM, so the tension remains, see Fig. 1. More specifically with SN+BAO+CMB, we get  $H_0 = 68.6 \pm 0.5$  which is in the  $4.4\sigma$  tail of the SH0ES team estimate.

We conclude that there is a drastic difference in the inferred value of  $H_0$  depending on whether BAOtr or 3D BAO is used. This indicates that the model dependence of the ordinary 3D BAO data can introduce a significant bias in  $H_0$ .

To understand why the bimetric model alleviates the tension when using BAOtr, we start by analyzing the  $\Lambda$ CDM model. First, SNIa data constrain the shape of the expansion history at redshifts  $z \leq 2.26$  while being agnostic to the absolute scale of the expansion rate ( $H_0$ ). Since the low-redshift expansion history is set by  $\Omega_\Lambda$  in a  $\Lambda$ CDM model, SNIa data constrain the value of  $\Omega_\Lambda$ . Further, the CMB angular scale  $\theta_{\text{CMB}}$  (3.4) is sensitive to the value of  $H_0$ . The observed value of  $\theta_{\text{CMB}}$  sets  $H_0$  to be relatively low, that is, in tension with SH0ES. In other words, increasing  $H_0$  to values compatible with SH0ES results in an increased angular scale  $\theta_{\text{CMB}}$ , violating its observational constraints.

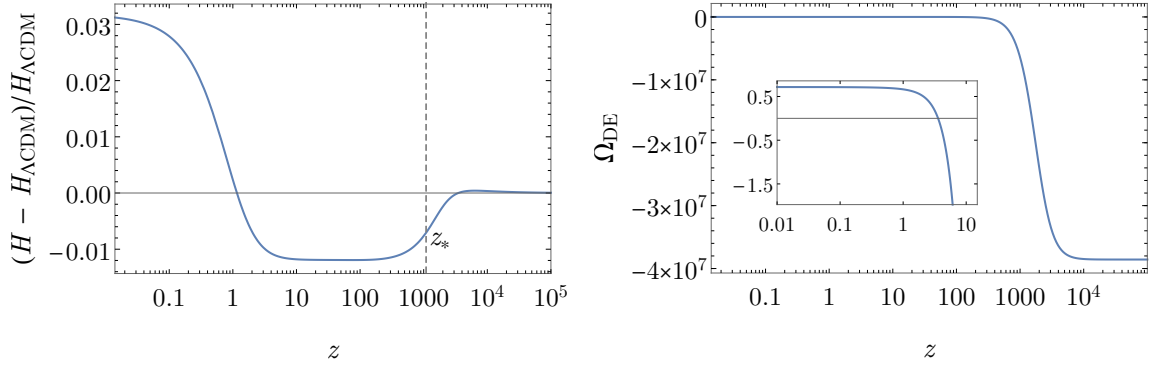


**Figure 2:** *Left:* Relative difference in the expansion rate  $H(z)$ , comparing the best-fit bimetric and  $\Lambda$ CDM models. The bimetric model exhibits  $(H_0, \theta, m_{\text{FP}}, \Omega_\Lambda, \alpha, \beta) = (71.0, 9.4^\circ, 5030, 0.724, 41, 46)$  and the  $\Lambda$ CDM model has  $(H_0, \Omega_\Lambda) = (68.9, 0.699)$ . *Right:* Dark energy density  $\Omega_{\text{DE}}$  for the same bimetric model. As apparent, there is a transition from a negative cosmological constant at high redshifts to a positive cosmological constant at lower redshifts.

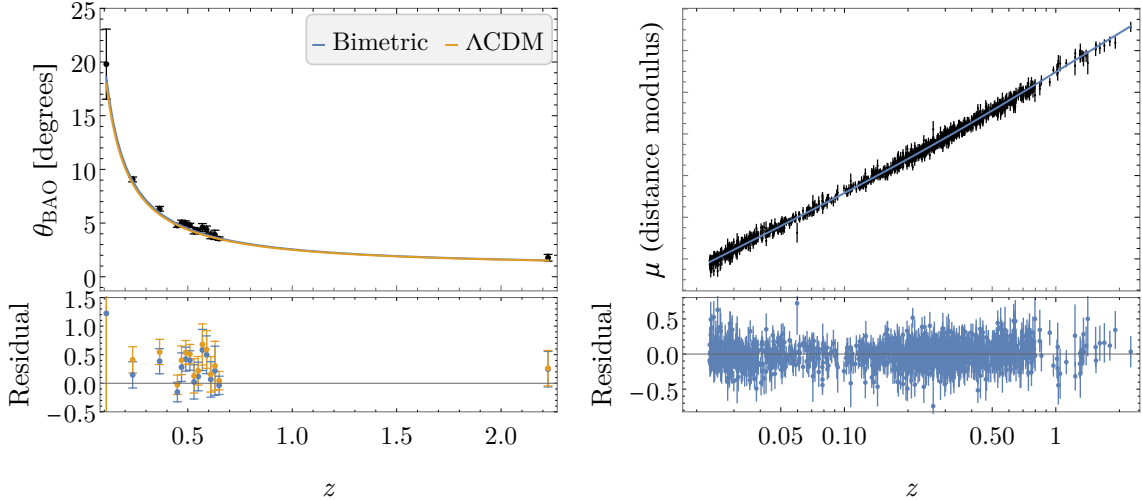


**Figure 3:** *Left:* Angular BAO scale for a bimetric model and a  $\Lambda$ CDM model. Data points are black. The bimetric model has the parameters  $(H_0, \theta, m_{\text{FP}}, \Omega_\Lambda, \alpha, \beta) = (71.0, 9.4^\circ, 5030, 0.724, 41, 46)$ . The  $\Lambda$ CDM model has  $(H_0, \Omega_\Lambda) = (68.9, 0.699)$ . By inspection, it can be seen that the  $\Lambda$ CDM residuals have a systematic offset. This offset is reduced in the bimetric model. *Right:* Distance modulus as a function of redshift for the same bimetric model. Since the SNIa data constrain only the shape of the distance modulus  $\mu$  rather its intercept on the  $y$ -axis, we do not specify the absolute scale of the  $y$ -axis.

However, this argument does not apply to bimetric cosmology due its increased flexibility. In this case, the expansion rate can be increased at small redshifts ( $z \lesssim 1$ ) while decreased at intermediate redshifts ( $1 \lesssim z \lesssim 1000$ ), compared with a  $\Lambda$ CDM model, so that the angular scale  $\theta_{\text{CMB}}$  is unchanged. An example is shown in Fig. 2 for the best-fit bimetric model. However, it remains to explain why bimetric cosmology, in combination with BAOtr, actually prefers a cosmology with an increased expansion rate in the late universe. To understand this,

in Fig. 3 we plot the angular BAO scale  $\theta_{\text{BAO}}$  for this model. Upon inspection of the residuals, it is evident that the  $\Lambda\text{CDM}$  model prediction lies systematically below the observed values. This can be remedied by increasing the expansion rate at these redshifts. However, in  $\Lambda\text{CDM}$  this is not possible due to the tight constraints on  $H_0$  from the CMB. In bimetric cosmology on the other hand, this is possible, as explained above. In short, BAOtr prefers an increased expansion rate in the late universe which can be accommodated in bimetric cosmology as opposed to  $\Lambda\text{CDM}$ . This is possible without spoiling CMB data due to a decrease in the expansion rate at intermediate redshifts.

With 3D BAO data on the other hand, there is no such offset between the  $\Lambda\text{CDM}$  model prediction and data. So, 3D BAO does not prefer an increased expansion rate at low redshifts, explaining the difference in  $H_0$  between BAOtr and 3D BAO. In summary, the choice of BAO data set (BAOtr or 3D BAO) effectively splits the SN+CMB confidence contour in Fig. 1 into two pieces with the model independent BAOtr piece being compatible with the SH0ES measurement and the 3D BAO piece assuming “low”  $H_0$  values in tension with SH0ES.

Finally, we check that the shape of the SH0ES-compatible bimetric expansion history is compatible with the SNIa data. To demonstrate this, in Fig. 3 we plot the distance modulus, defined as the difference between the apparent magnitude and the absolute magnitude,  $\mu = m - M$ . The theory prediction for this quantity is given by

$$\mu(z) = 5 \log_{10} \mathcal{D}_L(z) - 5 \log_{10} H_0 + 25. \quad (4.1)$$

As shown in Fig. 3, the bimetric model exhibits an expansion rate which is compatible also with SNIa data.

To quantify the degree of success of the bimetric model compared with  $\Lambda\text{CDM}$ , we assess the goodness-of-fit versus the number of model parameters. Two common measures of this are the Akaike information criterion (AIC) and the Bayesian information criterion (BIC) [76, 77]. The AIC is defined as

$$\text{AIC} = 2N_{\text{param}} + \chi_{\text{min}}^2. \quad (4.2)$$

The BIC approximates the Bayesian evidence and is defined as

$$\text{BIC} = N_{\text{param}} \ln N_{\text{data}} + \chi_{\text{min}}^2, \quad (4.3)$$

where  $N_{\text{param}}$  is the number of model parameters and  $N_{\text{data}}$  is the number of data points. Thus, the AIC and the BIC quantify how well a model is performing by balancing the goodness-of-fit of the model against its complexity, penalizing complex models that exhibit overfitting. In fact, the BIC exhibits a stronger penalty on models with more parameters compared with the AIC.

The degree to which one model is preferred over another is quantified by

$$\Delta\text{AIC} = \text{AIC}_{\Lambda\text{CDM}} - \text{AIC}_{\text{bimetric}}, \quad (4.4a)$$

$$\Delta\text{BIC} = \text{BIC}_{\Lambda\text{CDM}} - \text{BIC}_{\text{bimetric}}, \quad (4.4b)$$

so a positive value of  $\Delta\text{AIC}$  or  $\Delta\text{BIC}$  favours bimetric cosmology over  $\Lambda\text{CDM}$ , and vice versa.

As seen in Tab. 4, we are facing the ambiguous situation where the bimetric model is preferred by the AIC but the  $\Lambda\text{CDM}$  model is preferred by the BIC. If we focus on the inverse distance ladder (CMB+SN+BAOtr, i.e. without the SH0ES prior), there is a slight preference for the bimetric model according to the AIC whereas there is a strong preference for the  $\Lambda\text{CDM}$  model according to the BIC. Taken together, the two information criteria are

indecisive whereas to which model that exhibits the best performance. This demonstrates the limitations of the AIC and BIC in distinguishing between models. However, it should be stressed that the bimetric model has the advantage of the inverse distance ladder predicting a Hubble constant which is consistent with the local distance ladder measurement.

As seen in Fig. 2, the bimetric model alleviates the Hubble tension by increasing the expansion rate at low redshifts ( $z \lesssim 1$ ), compensating for this by a decreased expansion rate at intermediate redshifts ( $1 \lesssim z \lesssim 1000$ ) so that the CMB angular scale remains invariant. This expansion history is realized by the bimetric dark energy density  $\Omega_{\text{DE}}$  exhibiting a negative cosmological constant at high redshifts with a transition to a positive cosmological constant at low redshifts. In the example in Fig. 2,  $\Omega_{\text{DE}}$  is subdominant ( $< 1\%$ ) compared with  $\Omega_m$  at redshifts  $z \gtrsim 2000$  but yields a significant contribution to the expansion history at lower redshifts.

In Ref. [78] a similar cosmology was studied for a phenomenological model ( $\Lambda_s\text{CDM}$ ), exhibiting a similar transition between a negative and a positive cosmological constant. Similar to the results in the present paper, it was shown that the  $\Lambda_s\text{CDM}$  model yields a value for  $H_0$  which is compatible with SH0ES when using BAOtr data, thereby alleviating the tension. The main difference between bimetric cosmology and  $\Lambda_s\text{CDM}$  is that the latter introduces only one additional model parameter compared with the four in bimetric cosmology. This results in an unambiguous preference for  $\Lambda_s\text{CDM}$ , also by the BIC. On the other hand, bimetric cosmology presents a physically well-motivated framework for the  $\Lambda_s\text{CDM}$  model. As such, with  $\Omega_{\text{DE}}$  increasing with time, it constitutes a phantom dark energy. Since  $\Omega_{\text{DE}}$  mimics a cosmological constant also in the early universe, the bimetric modification to the expansion history can be ignored in the early universe. This can be seen in Fig. 2 as the expansion rate differs  $< 1\%$  at prerecombination redshifts  $z > z_*$ . This also means that the sound horizon at recombination and at the baryon drag epoch are the same as in the  $\Lambda\text{CDM}$  model.<sup>5</sup> Accordingly, with  $\theta_{\text{CMB}}$  fixed from observations, the distance to the last scattering surface  $D_A(z_*)$  also remains invariant.

## 5 Summary and discussion

In bimetric cosmology, the inverse distance ladder SN+BAOtr+CMB yields  $H_0 = 71.0 \pm 0.9$  which is compatible with SH0ES  $H_0 = 73.0 \pm 1.0$ , thus alleviating the Hubble tension. Here, we have used 2D transverse BAO data, eliminating the cosmological model dependence present in the ordinary BAO data. With ordinary 3D BAO data, bimetric cosmology eases the tension only very slightly, with a  $4.4\sigma$  tension remaining. Apparently, the choice between 2D BAO and 3D BAO makes a decisive difference with respect to the inferred value of  $H_0$ . With the more conservative option (BAOtr) alleviating the tension, this calls for further analysis of a possible bias in 3D BAO data. Ideally the 3D BAO data reduction should be redone assuming a bimetric cosmology. The goal of such an analysis would be to decrease the relatively large  $\sim 10\%$  errors in BAOtr to  $\sim 1\%$  errors as in the ordinary 3D BAO data, to see whether any Hubble tension-solving cosmologies remain. Such a re-analysis would likely be demanding but is nevertheless necessary to fully establish bimetric cosmology as an explanation of the Hubble tension.

The effectiveness of bimetric cosmology in alleviating the Hubble tension should also not be viewed in isolation. To be consistent, the theory parameters singled out by the inverse

<sup>5</sup>For the best-fit bimetric cosmology, shown in Fig. 2, the sound horizons are  $r_s(z_*) = 144.4\text{ Mpc}$  and  $r_s(z_d) = 147.0\text{ Mpc}$ .

distance ladder should describe a gravitational phenomenology in accordance with complementary tests of gravity. In Fig. 8.1 of Ref. [29], observational constraints from the following sources are compiled: solar-system tests, strong gravitational lensing (SGL) by galaxies, gravitational waves, and the abundance of the light elements (Big Bang nucleosynthesis).

With these additional probes, there remain viable regions in the parameter space in the range  $1 \lesssim m_{\text{FP}} \lesssim 10^4$ .<sup>6</sup> Interestingly, the allowed region overlaps with the region where the Hubble tension is alleviated. The lower limit  $m_{\text{FP}} \gtrsim 1$  is due to the Higuchi bound which is a theoretical requirement ensuring the absence of the Higuchi ghost [54]. The upper limit  $m_{\text{FP}} \lesssim 10^4$  is due to SGL. Recall that in the MCMC method, we set the likelihood to zero whenever there is no Vainshtein screening mechanism. In other words, the existence of a Vainshtein screening mechanism is guaranteed, making the region  $1 \lesssim m_{\text{FP}} \lesssim 10^4$  observationally viable.

As an example, with  $m_{\text{FP}} \sim 1000$ , the Vainshtein radius is  $r_V \sim 10$  kpc for a  $M = 10^{12} M_\odot$  galaxy, meaning that the typical lensing radius is of similar magnitude as the Vainshtein screening radius. This implies that  $m_{\text{FP}} \sim 1000$  is on the boundary of what is observational allowed by SGL. For a detailed analysis, see Ref. [79]. With future cosmological surveys such as Euclid, the sample size of strong gravitational lenses will increase by several orders of magnitude. This will probe larger portions of the parameter space (lower values of  $m_{\text{FP}}$ ) where the Hubble tension-solving models are located.

Another, less significant, tension that has gained interest recently is the tension between the observed distribution of galaxies predicted by CMB observations, assuming a  $\Lambda$ CDM cosmology, and for example large-scale structure surveys and weak lensing. This is quantified by the parameter  $S_8 = \sigma_8 \sqrt{\Omega_{m,0}}/0.3$  where  $\sigma_8$  is the present-day average amplitude of matter fluctuations at  $8h^{-1}$  Mpc. In bimetric cosmology, such as the model  $(H_0, \theta, m_{\text{FP}}, \Omega_\Lambda, \alpha, \beta) = (71.0, 9.4^\circ, 5030, 0.724, 41, 46)$  studied in Section 4, the present-day matter density  $\Omega_{m,0}$  is greater than in a  $\Lambda$ CDM model. For this model,  $\Omega_{m,0} = 0.284$ . The decrease in  $\Omega_{m,0}$  is due to the fact that  $\Omega_\Lambda$  is the effective cosmological constant that  $\Omega_{\text{DE}}$  approaches at future infinity, and thus assumes a greater value than the present-day value  $\Omega_{\text{DE},0}$ . With a decreased present-day matter density,  $S_8$  decreases, also easing the  $S_8$  tension, assuming that  $\sigma_8$  is constant. However, one should be very careful to draw such a conclusion at this stage since there is currently no framework that allows to predict structure formation in this theory [22, 57, 80–83]. So, at present we cannot justify the assumption of  $\sigma_8$  being unchanged in this theory.

We have focused on the most general bimetric model. In Tab. 5 and Tab. 6 in Appendix B, we present the corresponding results for all viable submodel, that is,  $B_0 B_1 B_2 B_3$ ,  $B_1 B_2 B_3 B_4$ , and  $B_1 B_2 B_3$ . The four-parameter model  $B_0 B_1 B_2 B_3$  is performing better than  $B_1 B_2 B_3 B_4$  with respect to the Hubble tension. Due to the decreased number of theory parameters, these models are slightly favoured over the general model when assessed by the BIC. The most restricted submodel ( $B_1 B_2 B_3$ ) on the other hand yields a Hubble constant which is in tension with SH0ES, just as the  $\Lambda$ CDM model.

---

<sup>6</sup>There are also windows of viable Fierz–Pauli masses in the ranges  $10^6 \lesssim m_{\text{FP}} \lesssim 10^8$  and  $m_{\text{FP}} \gtrsim 10^{32}$ .



## A Ratio of the scale factors: equation of motion

The quartic polynomial governing the evolution of  $y$ , the ratio of the scale factors, is given by,

$$\begin{aligned}
& -\frac{1}{3} \cos^2 \theta m_{\text{FP}}^2 (1 + 2\alpha + \beta) \\
& + \left[ \Omega_{\text{tot}}(z) + \Omega_{\Lambda} + m_{\text{FP}}^2 \left( \cos^2 \theta (\alpha + \beta) - \sin^2 \theta \left( 1 + \alpha + \frac{\beta}{3} \right) \right) \right] y(z) \\
& + m_{\text{FP}}^2 [-\cos^2 \theta \beta + \sin^2 \theta (1 + 2\alpha + \beta)] y^2(z) \\
& - \left[ \Omega_{\Lambda} + \frac{1}{3} m_{\text{FP}}^2 (\cos^2 \theta (-1 + \alpha - \beta) + 3 \sin^2 \theta (\alpha + \beta)) \right] y^3(z) \\
& + \frac{1}{3} \sin^2 \theta m_{\text{FP}}^2 \beta y^4(z) = 0,
\end{aligned} \tag{A.1}$$

where  $\Omega_{\text{tot}}(z) \equiv \Omega_m(z) + \Omega_r(z)$ . In the data analysis, we solve this equation numerically for each redshift, choosing the finite branch solution. That is, the solution satisfying  $0 \leq y \leq 1$ .

Evaluating eq. (A.1) and eq. (2.6) at  $z = 0$  (present day), the equations can be combined to yield an equation involving only  $y_0$  and the physical parameters. Here,  $y_0$  is the value of  $y$  at  $z = 0$ . The quartic term cancels and the equation reads,

$$\begin{aligned}
& \frac{1}{3} \cos^2 \theta m_{\text{FP}}^2 (1 + 2\alpha + \beta) - [1 + \cos^2 \theta m_{\text{FP}}^2 (\alpha + \beta)] y_0 + \cos^2 \theta m_{\text{FP}}^2 \beta y_0^2 \\
& + \left[ \Omega_{\Lambda} + \frac{1}{3} \cos^2 \theta m_{\text{FP}}^2 (-1 + \alpha - \beta) \right] y_0^3 = 0.
\end{aligned} \tag{A.2}$$

## B Complementary results

In Tab. 5 and Tab. 6 we display results complementary to Tab. 4, including the possible bimetric submodels  $B_0B_1B_2B_3$ ,  $B_1B_2B_3B_4$ , and  $B_1B_2B_3$ .

Model	CMB+SN+	$H_0$	$\theta$ (rad)	$\Omega_{\Lambda}$	$\Delta\text{AIC}$	$\Delta\text{BIC}$
$\Lambda\text{CDM}$	BAO	$68.3 \pm 0.4$	0	$0.691 \pm 0.005$	0	0
	BAOtr	$68.9 \pm 0.5$	0	$0.700 \pm 0.006$	0	0
$B_0B_1B_2B_3B_4$	BAO	$68.6 \pm 0.5$	$0.078 \pm 0.036$	$0.695 \pm 0.006$	-7.1	-28.0
	BAOtr	$71.0 \pm 0.9$	$0.163 \pm 0.028$	$0.724 \pm 0.010$	1.1	-19.9
$B_0B_1B_2B_3$	BAO	$68.5 \pm 0.6$	$0.088 \pm 0.040$	$0.695 \pm 0.007$	-3.8	-20.6
	BAOtr	$70.9 \pm 1.0$	$0.171 \pm 0.003$	$0.726 \pm 0.001$	3.0	-12.7
$B_1B_2B_3B_4$	BAO	$68.3 \pm 0.4$	$0.015 \pm 0.035$	$0.692 \pm 0.005$	-8.6	-21.3
	BAOtr	$69.3 \pm 0.8$	$0.1 \pm 0.073$	$0.707 \pm 0.013$	-2.6	-18.3
$B_1B_2B_3$	BAO	$68.2 \pm 0.4$	$10^{-3.56 \pm 0.88}$	$0.691 \pm 0.005$	-4.0	-14.5
	BAOtr	$68.9 \pm 0.5$	$10^{-3.50 \pm 0.90}$	$0.699 \pm 0.006$	-2.9	-13.4

**Table 5:** Best-fit values and 68% confidence errors for  $H_0$ ,  $\theta$ , and  $\Omega_{\Lambda}$  due to CMB+SN+BAO(tr) data.

Model	CMB+SN+	$H_0$	$\theta$ (rad)	$\Omega_\Lambda$	$\Delta\text{AIC}$	$\Delta\text{BIC}$
$\Lambda\text{CDM}$	BAO+SH0ES	$68.9 \pm 0.3$	0	$0.698 \pm 0.004$	0	0
	BAOtr+SH0ES	$69.7 \pm 0.5$	0	$0.709 \pm 0.006$	0	0
$B_0B_1B_2B_3B_4$	BAO+SH0ES	$69.4 \pm 0.5$	$0.119 \pm 0.031$	$0.704 \pm 0.006$	-1.8	-22.7
	BAOtr+SH0ES	$71.9 \pm 0.7$	$0.178 \pm 0.023$	$0.732 \pm 0.007$	13.2	-7.8
$B_0B_1B_2B_3$	BAO+SH0ES	$69.2 \pm 0.6$	$0.109 \pm 0.038$	$0.704 \pm 0.006$	0.2	-15.5
	BAOtr+SH0ES	$71.8 \pm 0.8$	$0.183 \pm 0.022$	$0.733 \pm 0.008$	15.0	-0.7
$B_1B_2B_3B_4$	BAO+SH0ES	$69.0 \pm 0.4$	$0.048 \pm 0.057$	$0.701 \pm 0.006$	-1.5	-17.2
	BAOtr+SH0ES	$70.6 \pm 0.7$	$0.173 \pm 0.067$	$0.723 \pm 0.010$	6.7	-9.0
$B_1B_2B_3$	BAO+SH0ES	$68.8 \pm 0.4$	$10^{-3.47 \pm 0.96}$	$0.698 \pm 0.005$	-2.6	-13.1
	BAOtr+SH0ES	$69.7 \pm 0.5$	$10^{-3.44 \pm 0.95}$	$0.709 \pm 0.006$	-1.0	-11.5

**Table 6:** Best-fit values and 68% confidence errors for  $H_0$ ,  $\theta$ , and  $\Omega_\Lambda$  due to CMB+SN+BAO(tr)+SH0ES. That is, including the  $H_0$  prior from SH0ES.

In Fig. 4-Fig. 7 we show the full 2D marginalized CL contours for all bimetric submodels, as well as the  $\Lambda\text{CDM}$  model in Fig. 8. As apparent in Fig. 4, the parameters  $\alpha$  and  $\beta$  are unconstrained when combining SN+BAO(tr)+CMB. Concerning the  $B_1B_2B_3$ -model, displayed in Fig. 7, we notice that the best-fit reduces to a  $\Lambda\text{CDM}$  model, that is,  $\theta \simeq 0$ . This explains the peak in the likelihood for  $m_{\text{FP}}$  towards higher values of  $m_{\text{FP}}$ . The reason is that for a  $B_1B_2B_3$ -model, the consistency constraints, discussed in Section 3.5, enforce a small value for  $\theta$  for large values of  $m_{\text{FP}}$ . This is discussed in detail in Section 3.2 in Ref. [27]. Moreover, in the  $\theta \rightarrow 0$  limit,  $\Lambda\text{CDM}$  is retained. So, a peak at large  $m_{\text{FP}}$  is consistent with  $\theta \simeq 0$  being the best-fit model. Already at  $m_{\text{FP}} \sim 100$ , it is required that  $\theta \lesssim 0.1^\circ$  for a  $B_1B_2B_3$ -model which, for all practical purposes, represents a  $\Lambda\text{CDM}$  model. Thus, it is not necessary to increase the parameter range in  $m_{\text{FP}}$ .

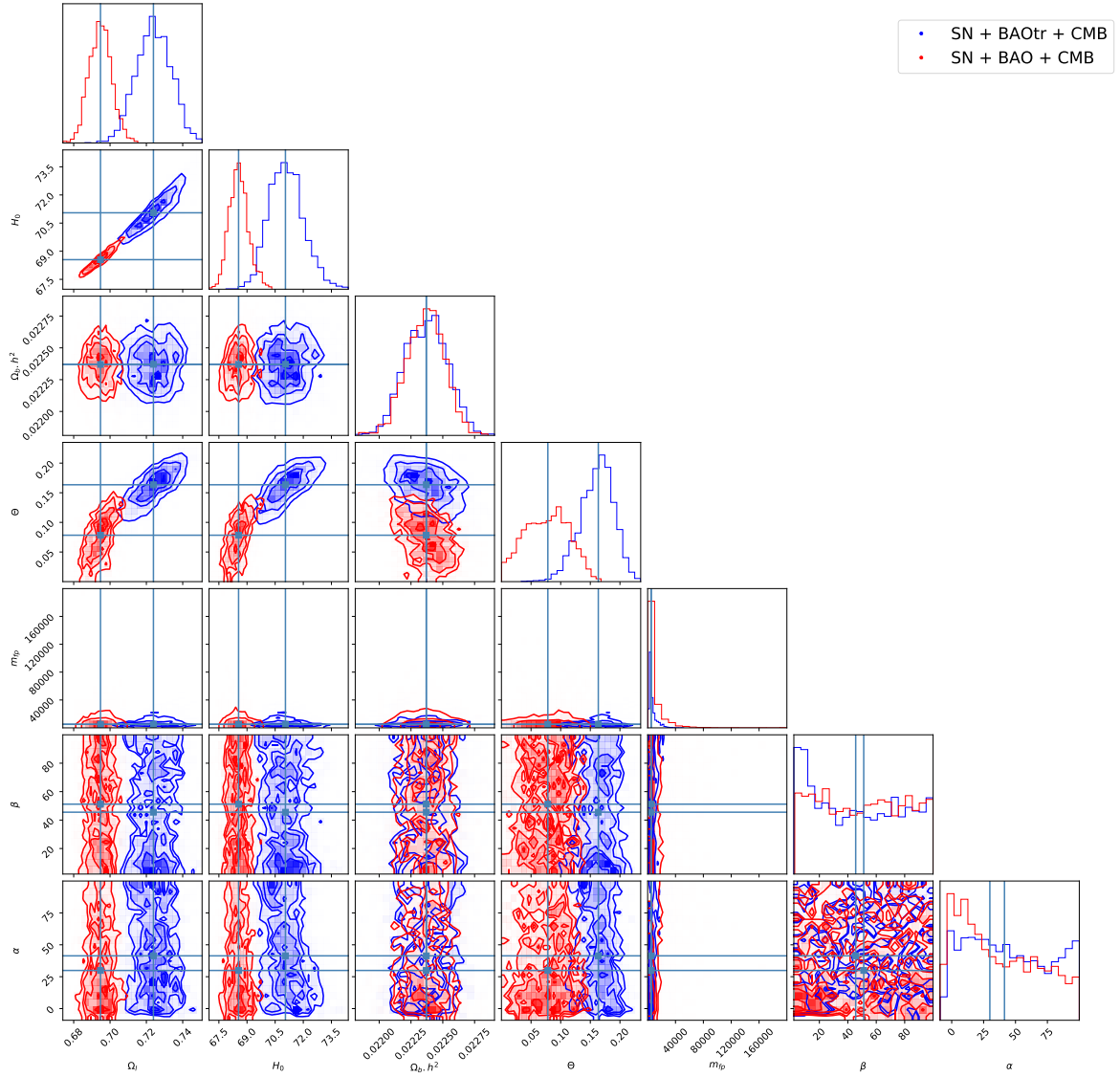


**Figure 4:** The corner plot shows the 2D marginalized CL contours for the most general bimetric model ( $B_0 B_1 B_2 B_3 B_4$ ). It is evident that the inclusion of BAOtr instead of ordinary 3D BAO results in a noticeable increment of the estimated value of the Hubble constant  $H_0$ .

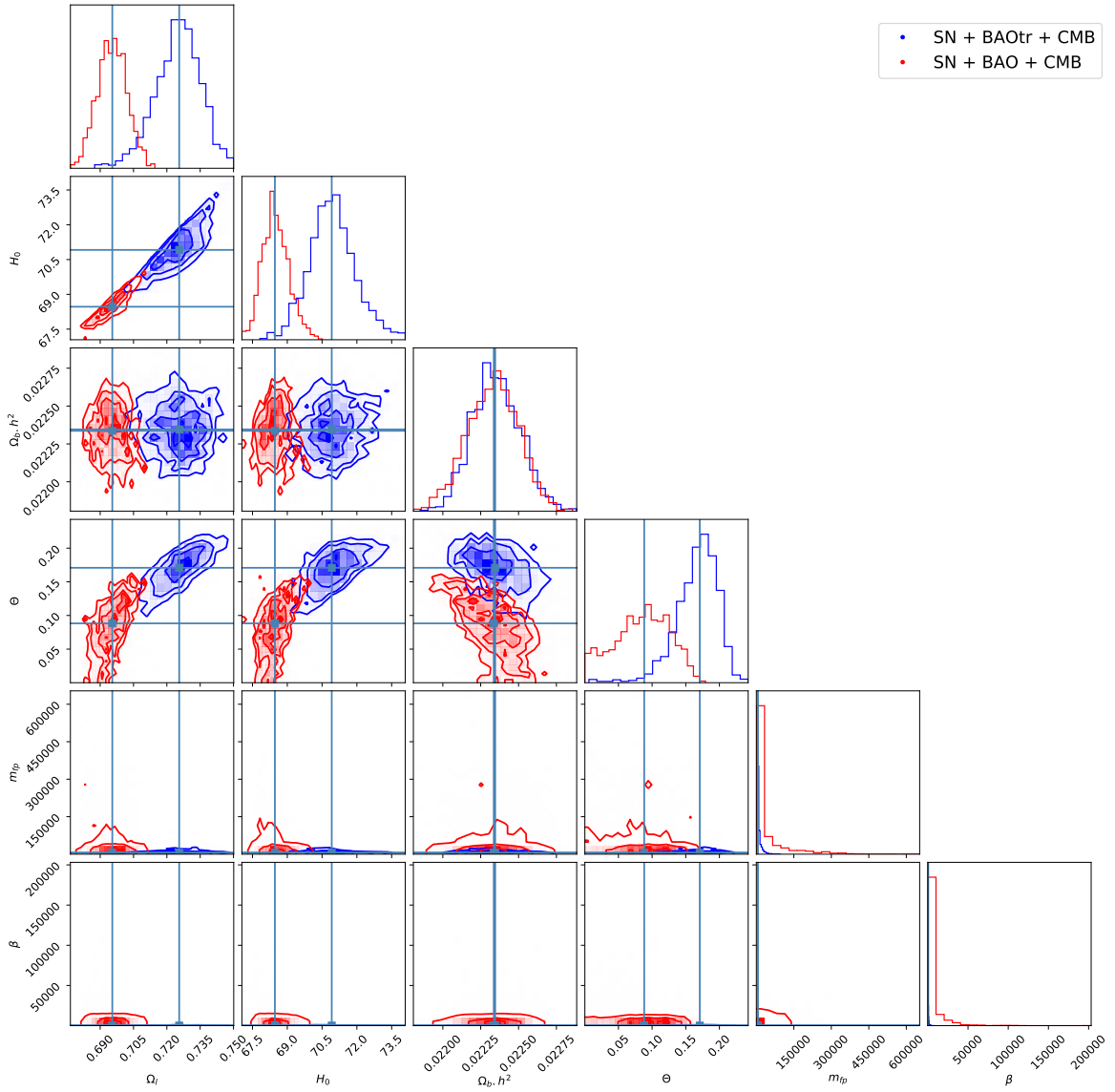


**Figure 5:** The  $B_0B_1B_2B_3$ -model. It is apparent that the inclusion of BAOtr instead of ordinary 3D BAO leads to a discernible increase in the estimated value of the Hubble constant  $H_0$ . In this four-parameter submodel,  $\alpha$  is not a free parameter but becomes dependent on the remaining physical parameters, which is why it is not shown in the plot.

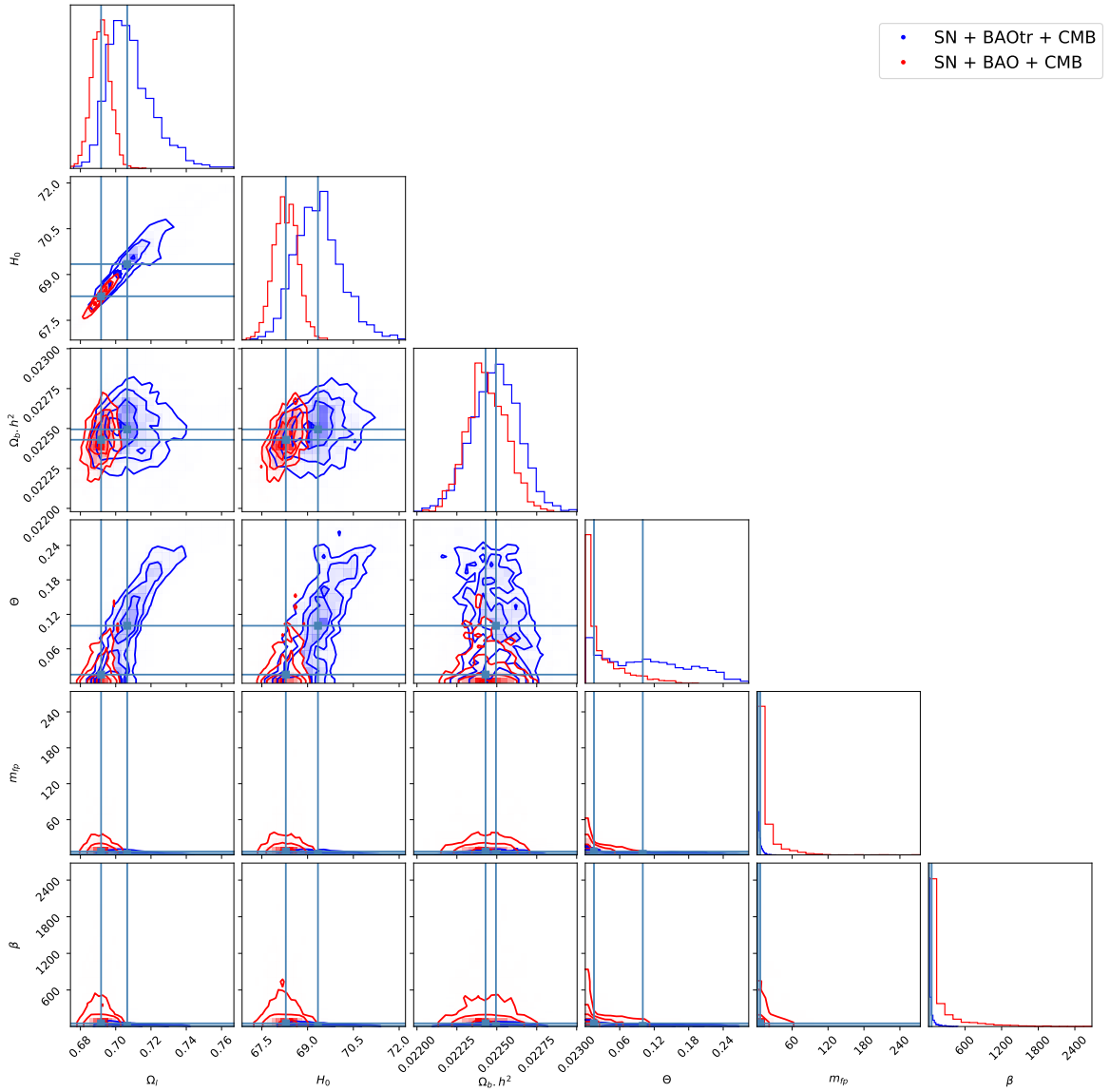


**Figure 6:** The  $B_1B_2B_3B_4$ -model. Incorporating BAOtr instead of ordinary 3D BAO results in a slight augmentation of the estimated value of the Hubble constant  $H_0$ . In this four-parameter submodel,  $\alpha$  is not a free parameter but becomes dependent on the remaining physical parameters, which is why it is not shown in the plot.

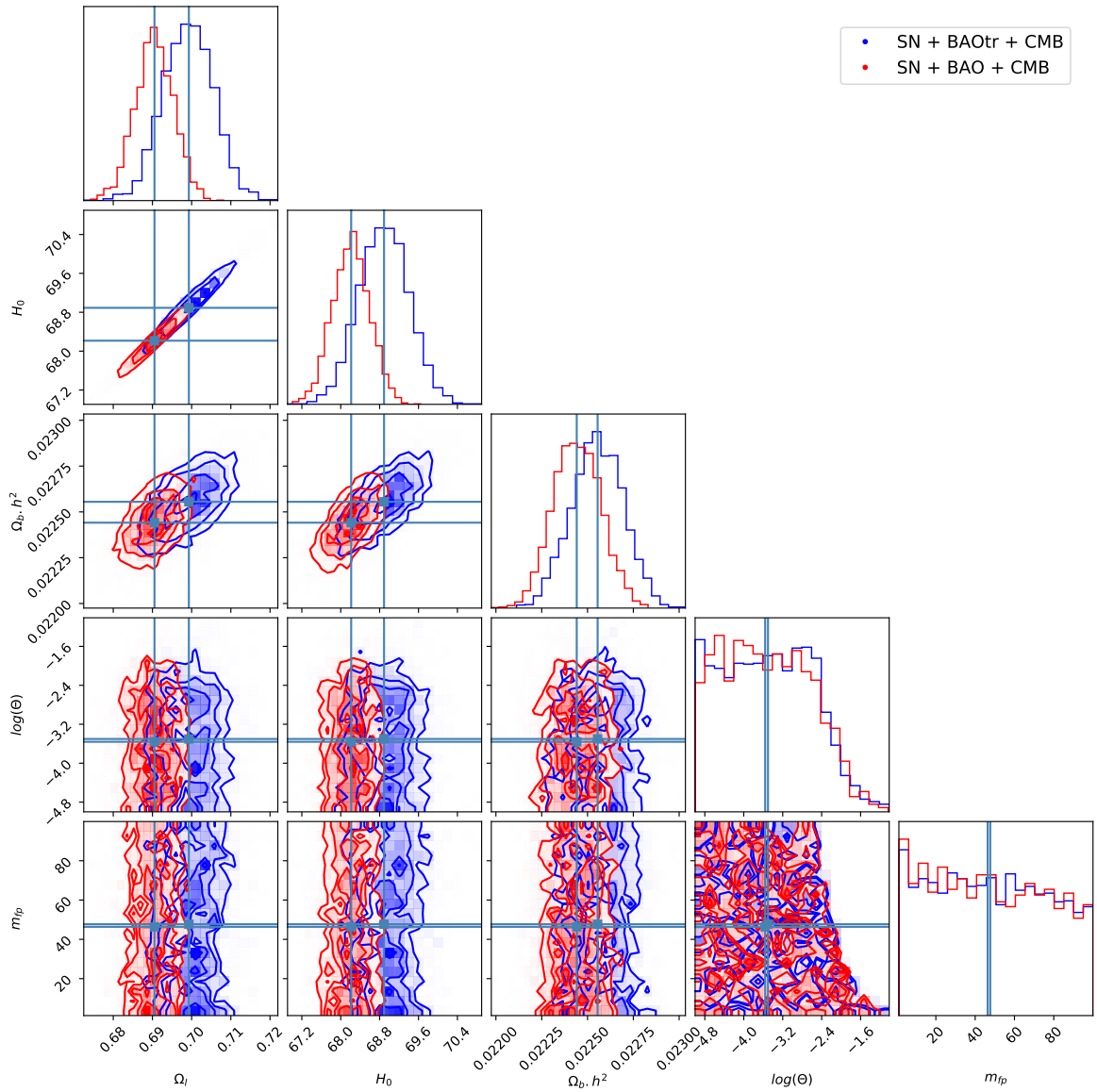


**Figure 7:** The  $B_1B_2B_3$ -model. The inclusion of BAOtr instead of ordinary 3D BAO leads to a slight increase in the estimated value of the Hubble constant  $H_0$ . In this three-parameter submodel,  $\alpha$  and  $\beta$  are not free parameters but become dependent on the remaining physical parameters, which is why they are not shown in the plot.

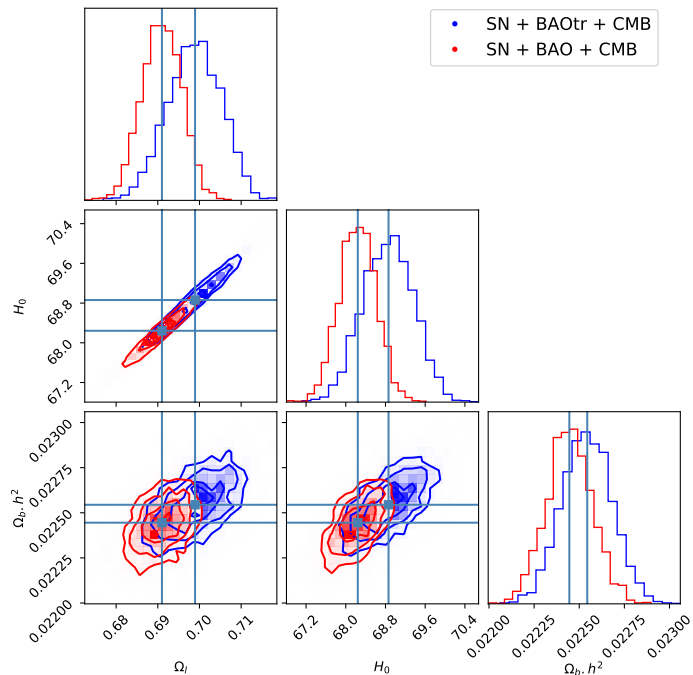


**Figure 8:** The corner plot shows the distribution of parameter values for a  $\Lambda$ CDM model. It is apparent that including BAOtr instead of ordinary 3D BAO leads to a slight increase in  $H_0$ . However, the increment does not suffice to solve the Hubble tension and, moreover, for  $\Lambda$ CDM, the usage of ordinary 3D BAO is warranted since the assumptions of the 3D BAO data reduction is compatible with such a cosmology.

## Acknowledgments

Thanks to Armando Bernui and Rafael Nunes for valuable discussions on 2D BAO data and the  $\Lambda_s$ CDM model. Special thanks to Edvard Mörtsell for valuable comments on the manuscript and fruitful discussions which led to significant improvements of the analysis.

## References

- [1] C. M. Will, *The Confrontation between General Relativity and Experiment*, *Living Rev. Rel.* **17** (2014) 4, [1403.7377].
- [2] A. G. Riess et al., *A Comprehensive Measurement of the Local Value of the Hubble Constant with 1 km s<sup>-1</sup> Mpc<sup>-1</sup> Uncertainty from the Hubble Space Telescope and the SH0ES Team*, *Astrophys. J. Lett.* **934** (2022) L7, [2112.04510].
- [3] PLANCK collaboration, N. Aghanim et al., *Planck 2018 results. VI. Cosmological parameters*, *Astron. Astrophys.* **641** (2020) A6, [1807.06209].
- [4] H. Desmond, B. Jain and J. Sakstein, *Local resolution of the Hubble tension: The impact of screened fifth forces on the cosmic distance ladder*, *Phys. Rev. D* **100** (2019) 043537, [1907.03778].
- [5] M. Höggås and E. Mörtsell, *Hubble tension and fifth forces*, *Phys. Rev. D* **108** (2023) 124050, [2309.01744].

- [6] M. Högås and E. Mörtzell, *Impact of symmetron screening on the Hubble tension: New constraints using cosmic distance ladder data*, *Phys. Rev. D* **108** (2023) 024007, [[2303.12827](#)].
- [7] E. Abdalla et al., *Cosmology intertwined: A review of the particle physics, astrophysics, and cosmology associated with the cosmological tensions and anomalies*, *JHEAp* **34** (2022) 49–211, [[2203.06142](#)].
- [8] N. Schöneberg, G. Franco Abellán, A. Pérez Sánchez, S. J. Witte, V. Poulin and J. Lesgourgues, *The  $H_0$  Olympics: A fair ranking of proposed models*, *Phys. Rept.* **984** (2022) 1–55, [[2107.10291](#)].
- [9] S. F. Hassan and R. A. Rosen, *Bimetric Gravity from Ghost-free Massive Gravity*, *JHEP* **02** (2012) 126, [[1109.3515](#)].
- [10] S. F. Hassan, A. Schmidt-May and M. von Strauss, *On Consistent Theories of Massive Spin-2 Fields Coupled to Gravity*, *JHEP* **05** (2013) 086, [[1208.1515](#)].
- [11] M. von Strauss, A. Schmidt-May, J. Enander, E. Mortsell and S. F. Hassan, *Cosmological Solutions in Bimetric Gravity and their Observational Tests*, *JCAP* **03** (2012) 042, [[1111.1655](#)].
- [12] S. Sjors and E. Mortsell, *Spherically Symmetric Solutions in Massive Gravity and Constraints from Galaxies*, *JHEP* **02** (2013) 080, [[1111.5961](#)].
- [13] Y. Akrami, T. S. Koivisto and M. Sandstad, *Accelerated expansion from ghost-free bigravity: a statistical analysis with improved generality*, *JHEP* **03** (2013) 099, [[1209.0457](#)].
- [14] J. Enander and E. Mörtzell, *Strong lensing constraints on bimetric massive gravity*, *JHEP* **10** (2013) 031, [[1306.1086](#)].
- [15] E. Babichev and M. Crisostomi, *Restoring general relativity in massive bigravity theory*, *Phys. Rev. D* **88** (2013) 084002, [[1307.3640](#)].
- [16] F. Koennig, A. Patil and L. Amendola, *Viable cosmological solutions in massive bimetric gravity*, *JCAP* **03** (2014) 029, [[1312.3208](#)].
- [17] J. Enander and E. Mortsell, *On stars, galaxies and black holes in massive bigravity*, *JCAP* **11** (2015) 023, [[1507.00912](#)].
- [18] K. Max, M. Platscher and J. Smirnov, *Gravitational Wave Oscillations in Bigravity*, *Phys. Rev. Lett.* **119** (2017) 111101, [[1703.07785](#)].
- [19] S. Dhawan, A. Goobar, E. Mörtzell, R. Amanullah and U. Feindt, *Narrowing down the possible explanations of cosmic acceleration with geometric probes*, *JCAP* **07** (2017) 040, [[1705.05768](#)].
- [20] M. Platscher, J. Smirnov, S. Meyer and M. Bartelmann, *Long Range Effects in Gravity Theories with Vainshtein Screening*, *JCAP* **12** (2018) 009, [[1809.05318](#)].
- [21] M. Lüben, E. Mörtzell and A. Schmidt-May, *Bimetric cosmology is compatible with local tests of gravity*, *Class. Quant. Grav.* **37** (2020) 047001, [[1812.08686](#)].
- [22] M. Högås, F. Torsello and E. Mörtzell, *On the stability of bimetric structure formation*, *JCAP* **04** (2020) 046, [[1910.01651](#)].
- [23] M. Lüben, A. Schmidt-May and J. Weller, *Physical parameter space of bimetric theory and  $SN_{Ia}$  constraints*, *JCAP* **09** (2020) 024, [[2003.03382](#)].
- [24] M. Lindner, K. Max, M. Platscher and J. Rezaeck, *Probing alternative cosmologies through the inverse distance ladder*, *JCAP* **10** (2020) 040, [[2002.01487](#)].
- [25] A. Caravano, M. Lüben and J. Weller, *Combining cosmological and local bounds on bimetric theory*, *JCAP* **09** (2021) 035, [[2101.08791](#)].
- [26] M. Högås and E. Mörtzell, *Constraints on bimetric gravity. Part I. Analytical constraints*, *JCAP* **05** (2021) 001, [[2101.08794](#)].



- [27] M. Högås and E. Mörtzell, *Constraints on bimetric gravity. Part II. Observational constraints*, *JCAP* **05** (2021) 002, [[2101.08795](#)].
- [28] M. Högås and E. Mörtzell, *Constraints on bimetric gravity from Big Bang nucleosynthesis*, *JCAP* **11** (2021) 001, [[2106.09030](#)].
- [29] M. Högås, *Was Einstein Wrong? : Theoretical and observational constraints on massive gravity*. PhD thesis, Stockholm University, Faculty of Science, Department of Physics, 2022.
- [30] M. S. Volkov, *Cosmological solutions with massive gravitons in the bigravity theory*, *JHEP* **01** (2012) 035, [[1110.6153](#)].
- [31] D. Comelli, M. Crisostomi, F. Nesti and L. Pilo, *FRW Cosmology in Ghost Free Massive Gravity*, *JHEP* **03** (2012) 067, [[1111.1983](#)].
- [32] M. S. Volkov, *Hairy black holes in the ghost-free bigravity theory*, *Phys. Rev. D* **85** (2012) 124043, [[1202.6682](#)].
- [33] M. S. Volkov, *Exact self-accelerating cosmologies in the ghost-free massive gravity – the detailed derivation*, *Phys. Rev. D* **86** (2012) 104022, [[1207.3723](#)].
- [34] M. S. Volkov, *Self-accelerating cosmologies and hairy black holes in ghost-free bigravity and massive gravity*, *Class. Quant. Grav.* **30** (2013) 184009, [[1304.0238](#)].
- [35] K. Aoki and S. Mukohyama, *Massive gravitons as dark matter and gravitational waves*, *Phys. Rev. D* **94** (2016) 024001, [[1604.06704](#)].
- [36] E. Babichev, L. Marzola, M. Raidal, A. Schmidt-May, F. Urban, H. Veermäe et al., *Heavy spin-2 Dark Matter*, *JCAP* **09** (2016) 016, [[1607.03497](#)].
- [37] E. Babichev, L. Marzola, M. Raidal, A. Schmidt-May, F. Urban, H. Veermäe et al., *Bigravitational origin of dark matter*, *Phys. Rev. D* **94** (2016) 084055, [[1604.08564](#)].
- [38] E. Mörtzell and S. Dhawan, *Does the Hubble constant tension call for new physics?*, *JCAP* **09** (2018) 025, [[1801.07260](#)].
- [39] M. Fierz and W. Pauli, *On relativistic wave equations for particles of arbitrary spin in an electromagnetic field*, *Proc. Roy. Soc. Lond. A* **173** (1939) 211–232.
- [40] D. G. Boulware and S. Deser, *Can gravitation have a finite range?*, *Phys. Rev. D* **6** (1972) 3368–3382.
- [41] G. Gabadadze, *General Relativity With An Auxiliary Dimension*, *Phys. Lett. B* **681** (2009) 89–95, [[0908.1112](#)].
- [42] C. de Rham, *Massive gravity from Dirichlet boundary conditions*, *Phys. Lett. B* **688** (2010) 137–141, [[0910.5474](#)].
- [43] C. de Rham and G. Gabadadze, *Self-tuned Massive Spin-2*, *Phys. Lett. B* **693** (2010) 334–338, [[1006.4367](#)].
- [44] C. de Rham and G. Gabadadze, *Generalization of the Fierz-Pauli Action*, *Phys. Rev. D* **82** (2010) 044020, [[1007.0443](#)].
- [45] C. de Rham, G. Gabadadze and A. J. Tolley, *Resummation of Massive Gravity*, *Phys. Rev. Lett.* **106** (2011) 231101, [[1011.1232](#)].
- [46] S. F. Hassan and R. A. Rosen, *On Non-Linear Actions for Massive Gravity*, *JHEP* **07** (2011) 009, [[1103.6055](#)].
- [47] S. F. Hassan and R. A. Rosen, *Confirmation of the Secondary Constraint and Absence of Ghost in Massive Gravity and Bimetric Gravity*, *JHEP* **04** (2012) 123, [[1111.2070](#)].
- [48] S. F. Hassan and A. Lundkvist, *Analysis of constraints and their algebra in bimetric theory*, *JHEP* **08** (2018) 182, [[1802.07267](#)].

- [49] C. de Rham, L. Heisenberg and R. H. Ribeiro, *On couplings to matter in massive (bi-)gravity*, *Class. Quant. Grav.* **32** (2015) 035022, [[1408.1678](#)].
- [50] C. de Rham, L. Heisenberg and R. H. Ribeiro, *Ghosts and matter couplings in massive gravity, bigravity and multigravity*, *Phys. Rev. D* **90** (2014) 124042, [[1409.3834](#)].
- [51] S. F. Hassan and M. Kocic, *On the local structure of spacetime in ghost-free bimetric theory and massive gravity*, *JHEP* **05** (2018) 099, [[1706.07806](#)].
- [52] N. Higham, *Functions of Matrices: Theory and Computation*. Society for Industrial and Applied Mathematics (SIAM, 3600 Market Street, Floor 6, Philadelphia, PA 19104), 2008.
- [53] G. W. Horndeski, *Second-order scalar-tensor field equations in a four-dimensional space*, *Int. J. Theor. Phys.* **10** (1974) 363–384.
- [54] A. Higuchi, *Forbidden Mass Range for Spin-2 Field Theory in De Sitter Space-time*, *Nucl. Phys. B* **282** (1987) 397–436.
- [55] M. Fasiello and A. J. Tolley, *Cosmological Stability Bound in Massive Gravity and Bigravity*, *JCAP* **12** (2013) 002, [[1308.1647](#)].
- [56] A. De Felice, A. E. Gümrükçüoğlu, S. Mukohyama, N. Tanahashi and T. Tanaka, *Viable cosmology in bimetric theory*, *JCAP* **06** (2014) 037, [[1404.0008](#)].
- [57] F. Könnig, *Higuchi Ghosts and Gradient Instabilities in Bimetric Gravity*, *Phys. Rev. D* **91** (2015) 104019, [[1503.07436](#)].
- [58] E. Mortsell, *Cosmological histories in bimetric gravity: A graphical approach*, *JCAP* **02** (2017) 051, [[1701.00710](#)].
- [59] A. De Felice, F. Larrouturou, S. Mukohyama and M. Oliosi, *Minimal Theory of Bigravity: construction and cosmology*, *JCAP* **04** (2021) 015, [[2012.01073](#)].
- [60] H. S. Leavitt and E. C. Pickering, *Periods of 25 Variable Stars in the Small Magellanic Cloud*, *Harvard Obs. Circ.* **173** (1912) 1–3.
- [61] A. G. Riess et al., *Milky Way Cepheid Standards for Measuring Cosmic Distances and Application to Gaia DR2: Implications for the Hubble Constant*, *Astrophys. J.* **861** (2018) 126, [[1804.10655](#)].
- [62] A. G. Riess, S. Casertano, W. Yuan, J. B. Bowers, L. Macri, J. C. Zinn et al., *Cosmic Distances Calibrated to 1% Precision with Gaia EDR3 Parallaxes and Hubble Space Telescope Photometry of 75 Milky Way Cepheids Confirm Tension with  $\Lambda$ CDM*, *Astrophys. J. Lett.* **908** (2021) L6, [[2012.08534](#)].
- [63] M. J. Reid, D. W. Pesce and A. G. Riess, *An Improved Distance to NGC 4258 and its Implications for the Hubble Constant*, *Astrophys. J. Lett.* **886** (2019) L27, [[1908.05625](#)].
- [64] G. Pietrzyński et al., *A distance to the Large Magellanic Cloud that is precise to one per cent*, *Nature* **567** (2019) 200–203.
- [65] D. Scolnic et al., *The Pantheon+ Analysis: The Full Data Set and Light-curve Release*, *Astrophys. J.* **938** (2022) 113, [[2112.03863](#)].
- [66] G. Efstathiou and J. R. Bond, *Cosmic confusion: Degeneracies among cosmological parameters derived from measurements of microwave background anisotropies*, *Mon. Not. Roy. Astron. Soc.* **304** (1999) 75–97, [[astro-ph/9807103](#)].
- [67] W. Hu and N. Sugiyama, *Small scale cosmological perturbations: An Analytic approach*, *Astrophys. J.* **471** (1996) 542–570, [[astro-ph/9510117](#)].
- [68] L. Chen, Q.-G. Huang and K. Wang, *Distance Priors from Planck Final Release*, *JCAP* **02** (2019) 028, [[1808.05724](#)].

- [69] M. Goliath, R. Amanullah, P. Astier, A. Goobar and R. Pain, *Supernovae and the nature of the dark energy*, *Astron. Astrophys.* **380** (2001) 6–18, [[astro-ph/0104009](#)].
- [70] R. C. Nunes, S. K. Yadav, J. F. Jesus and A. Bernui, *Cosmological parameter analyses using transversal BAO data*, *Mon. Not. Roy. Astron. Soc.* **497** (2020) 2133–2141, [[2002.09293](#)].
- [71] R. C. Nunes and A. Bernui, *BAO signatures in the 2-point angular correlations and the Hubble tension*, *Eur. Phys. J. C* **80** (2020) 1025, [[2008.03259](#)].
- [72] A. Bernui, E. Di Valentino, W. Giarè, S. Kumar and R. C. Nunes, *Exploring the  $H_0$  tension and the evidence for dark sector interactions from 2D BAO measurements*, *Phys. Rev. D* **107** (2023) 103531, [[2301.06097](#)].
- [73] DESI collaboration, A. G. Adame et al., *DESI 2024 VI: Cosmological Constraints from the Measurements of Baryon Acoustic Oscillations*, [2404.03002](#).
- [74] D. Foreman-Mackey, D. W. Hogg, D. Lang and J. Goodman, *emcee: The MCMC Hammer*, *Publ. Astron. Soc. Pac.* **125** (2013) 306, [[1202.3665](#)].
- [75] J. Goodman and J. Weare, *Ensemble samplers with affine invariance*, *Commun. Appl. Math. Comput. Sci.* **5** (2010) 65 – 80.
- [76] H. Akaike, *A new look at the statistical model identification*, *IEEE Trans. Automatic Control* **19** (1974) 716–723.
- [77] G. Schwarz, *Estimating the Dimension of a Model*, *Annals Statist.* **6** (1978) 461–464.
- [78] O. Akarsu, E. Di Valentino, S. Kumar, R. C. Nunes, J. A. Vazquez and A. Yadav,  *$\Lambda_s$  CDM model: A promising scenario for alleviation of cosmological tensions*, [2307.10899](#).
- [79] S. Guerrini and E. Mörtzell, *Probing a scale dependent gravitational slip with galaxy strong lensing systems*, *Phys. Rev. D* **109** (2024) 023533, [[2309.11915](#)].
- [80] K. Aoki, K.-i. Maeda and R. Namba, *Stability of the Early Universe in Bigravity Theory*, *Phys. Rev. D* **92** (2015) 044054, [[1506.04543](#)].
- [81] E. Mortsell and J. Enander, *Scalar instabilities in bimetric gravity: The Vainshtein mechanism and structure formation*, *JCAP* **10** (2015) 044, [[1506.04977](#)].
- [82] Y. Akrami, S. F. Hassan, F. Könnig, A. Schmidt-May and A. R. Solomon, *Bimetric gravity is cosmologically viable*, *Phys. Lett. B* **748** (2015) 37–44, [[1503.07521](#)].
- [83] M. Lüben, A. Schmidt-May and J. Smirnov, *Vainshtein Screening in Bimetric Cosmology*, *Phys. Rev. D* **102** (2020) 123529, [[1912.09449](#)].